Title Goes Here

true true

17 febrero, 2021

Contents

1 Introduction

2 Data & Methods

The phase of principal components is defined up to an additive constant. For real principal components, this constant can be either 0 or π, corresponding to a change in sign. For complex principal components, it can be any number between 0 and 2π (Horel, 1984). In this paper we chose the phase of each of the two complex principal components so that the real and imaginary part are easier to interpret. For the first complex principal component, the phase was chosen so that the time series corresponding to the imaginary part had a time mean of zero.

For the second complex principal component, the phase was chosen so that the coefficent of determination between the Oceanic Niño Index (Bamston et al., 1997) and the real part was minimised. It's important to reassure the reader that this procedure does not create a spurious correlation, it only takes whatever relationship that already exist and aligns it with a specific phase. If the relationship is very weak, the rotation cannot generate a strong relationship.

ERA5, ERA5 BE,

Table 1: R^2 between pairs of EOFs of each level rounded to two decimals.

	50 hPa			
200 hPa	EOF1	EOF2	EOF3	EOF4
EOF1	0.31	0.02	0.03	0.00
EOF2	0.00	0.02	0.74	0.01
EOF3	0.00	0.04	0.02	0.56
EOF4	0.08	0.06	0.01	0.16

Table 2: R^2 of the absolute magnitude of complex EOFs between 200 hPa and 50 hPa computing EOF separatedly for each level. The high correlation between levels for the two leading EOFs justifies treating the pattern as a mode of covariability between the stratosphere and the troposphere and, thus, computing the EOFs using both levels at the same time.

	50 hPa		
200 hPa	PC1	PC2	PC3
PC1	0.28	0.02	0.02
PC2	0.00	0.60	0.02
PC3	0.00	0.00	0.01

3 Results

No mostrar los EOFs no complejos. No tiene sentido mostralos si no se analizas.

Relacionar 50hPa con vórtice polar? Temperatura también suma. En 50 el negativo es más intenso que el negativo. ¿Por qué?

Ver qué pasa con U con el EOF1.

En 200 no se ve la señal de jet de la temperatura ¿qué pasa más abajo? en 700 la anomalía de temp coincide más o menos con el geopotential

Mostrar EOF espaciales.

Pp, ¿cuál es la regresión con SAM asim en 200 hPa?

Figure 16a show the spatial pattern of the 4 leading EOF of zonal anomalies of geopotential height for 50 hPa and 200 hPa computed separately. The percentages XXX . At 50 hPa, EOF1 and EOF2 on one hand, and EOF3 and EOF4 on the other are clearly pairs of zonal waves with wave numbers 1 and 2-3 respectively shifted by 1/4 wavelength. That is, each group of two EOFs represents the same zonal wave structure that changes in magnitude and location. Similarly, at 200 hPa EOF2 and EOF3 represent the same zonal wave structure with wave number ~3.

Furthermore, the wave 1 pattern represented by the first two EOFs at 50 hPa is similar to the wave 1 pattern shown as the leading EOF at 200 hPa, and the wave 2-3 pattern represented by the third and fourth EOF at 50 hPa is similar to the wave 3 pattern present in EOF2 and EOF3 at 200 hPa. These similarities suggest some level of joint variability across levels. Figure 16b shows the coefficient of determination between temporal series of each EOF at each level. EOF3 and EOF4 at 50 hPa are highly correlated with EOF2 and EOF3 at 200 hPa. Not only each pair of EOFs represent a single structure within each level, but they represent a coherent pattern of variability between levels. Similarly, the leading EOF of each level are relatively highly correlated, again suggesting an unique mode of joint variability.

Both observations motivate the decision of performing complex EOF jointly between levels. The computation of the EOFs was carried out using data from both levels at the same time, therefore, each complex EOF has a spatial part that depends on longitude, latitude and level, an a temporal part that depends only on time.

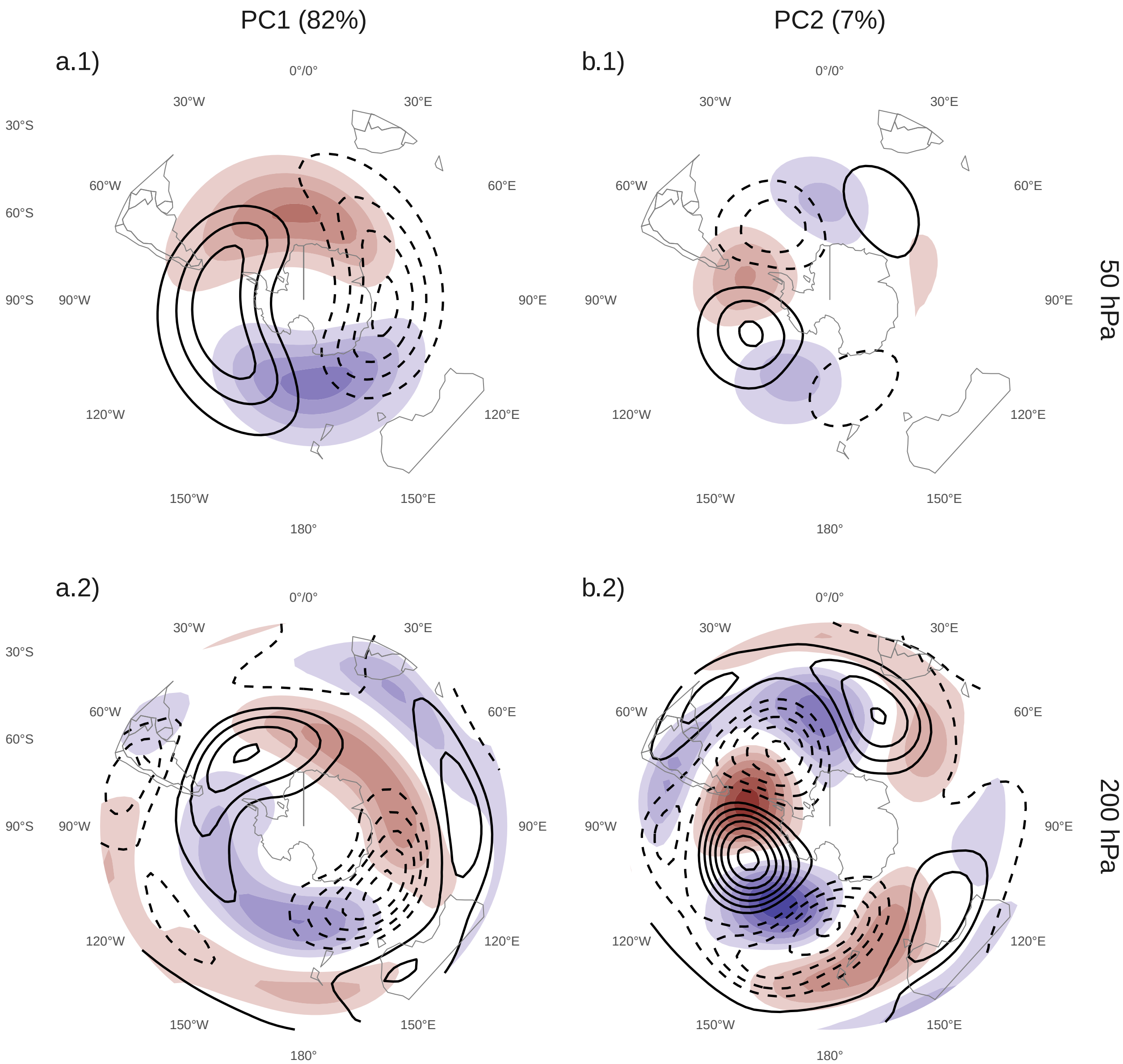

(a) Spatial patterns. Real part in shading, imaginary part in contours.

(b) Temproal series

Figures 1a and 1b show, respectively, the spatial and temporal parts of the first two leading complex EOFs of zonal anomalies of geopotential height at 50 hPa and 200 hPa. In the spatial patterns in Figure 1a, the real (in shading) and the imaginary parts (in contour) are in quadrature by construction, so that each EOF describe a single wave-like pattern whose amplitude and position (i.e. phase) is controlled by the magnitude and argument of the complex temporal EOF.

The wave patterns described by these complex EOFs match the patterns seen in the navie EOFs of Figure @ref(fig: cor-eof-naive-1): The first is a wave 1, while the second is a wave 3. Note that in Figure 1b, the real part of EOF1 has non zero mean. This is due to th fact that the geopotential fields that enter into the algorithm are anomalies with respect to the zonal mean (shown in Figure **??**), not the time mean. The real part of the first EOF is, therefore, capturing the mean zonally anomalous field and the variability that projects onto it.

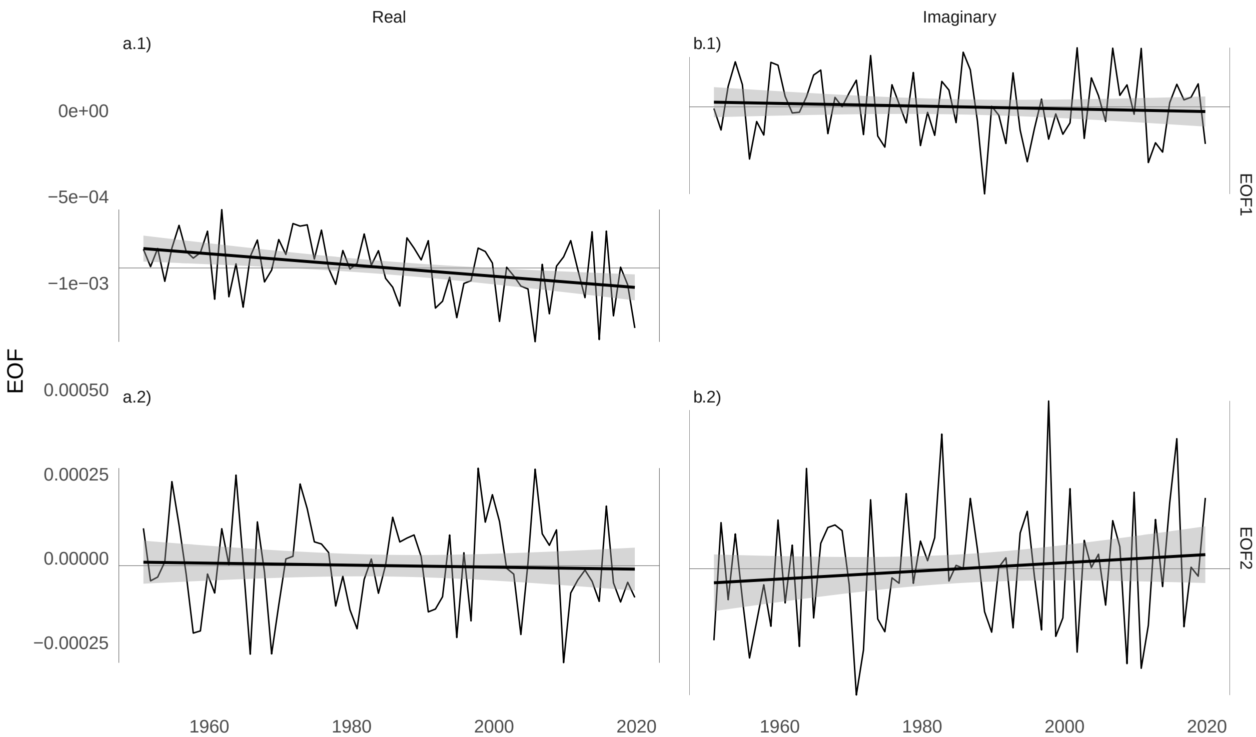

Figure 2: Temporal series extended using ERA5 back extended preliminary edition (period 1950 – 1978) and ERA5 (period 1979 – 2019). Each series is computed by projecting monthly geopotential height zonal anomalies standardised by level south of 20ºS onto the corresponding spatial pattern.

Figure 2 shows temporal series of the two complex EOFs extended beyond the satellite era using the preliminary ERA5 back extension going back to 1950 (which we call the "hybrid ERA5" reanalysis). There is a downward trend in the real part of EOF1 in the hybrid reanalysis (Figure 2a.1, p-value < 0.001). There is no significant trend in any of the complex parts of EOF2.

3.1 Regression

Figure 3 shows regression patterns of SON geopotential height on the real and imaginary part of the first EOF at 50 hPa and 200 hPa.

Interpretaciones:

- Parte real de EOF1: variabilidady que se proyecta en la dirección del campo medio
- Parte imaginaria de EOF1: variabilidad asociada a la parte simétrica del SAM

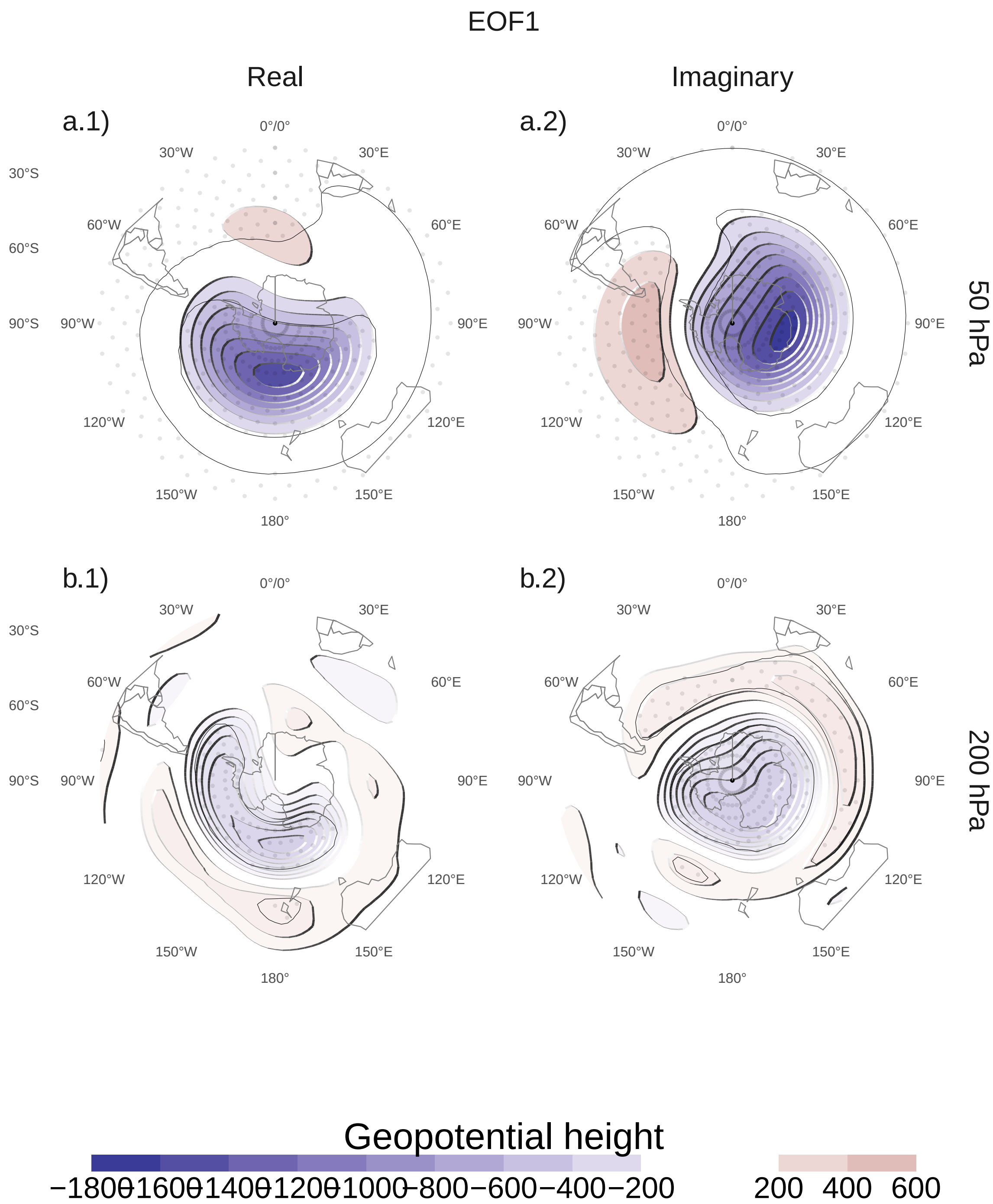

Figure 3: Regression coefficients of the real and imaginary part of the first complex EOF on SON geopotential height for the 1979 – 2019 period. These coefficients come from multiple linear regression involving the real and imaginary part of both EFO2.

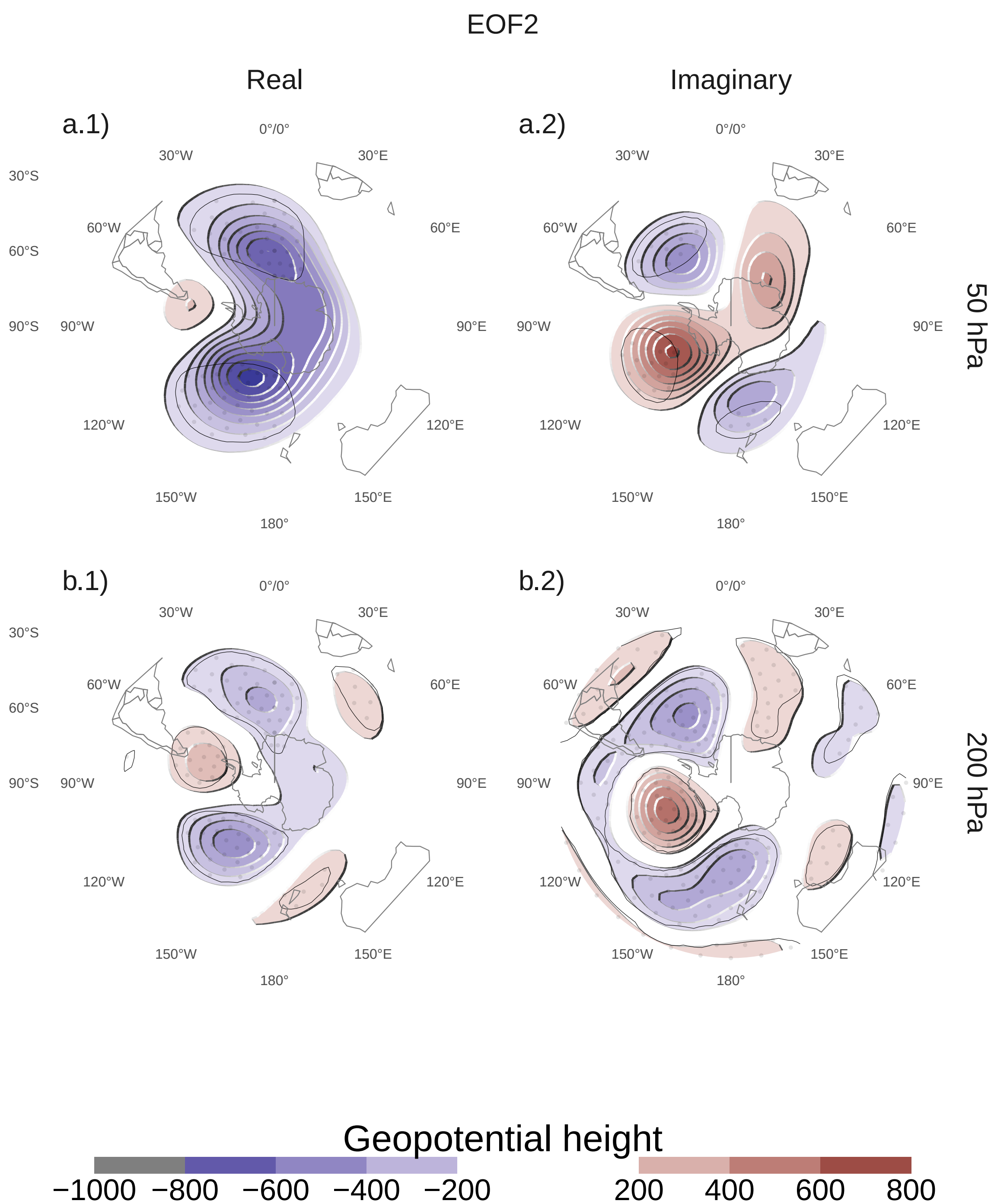

Figure 4: Same as Figure 3 but for the second EOF.

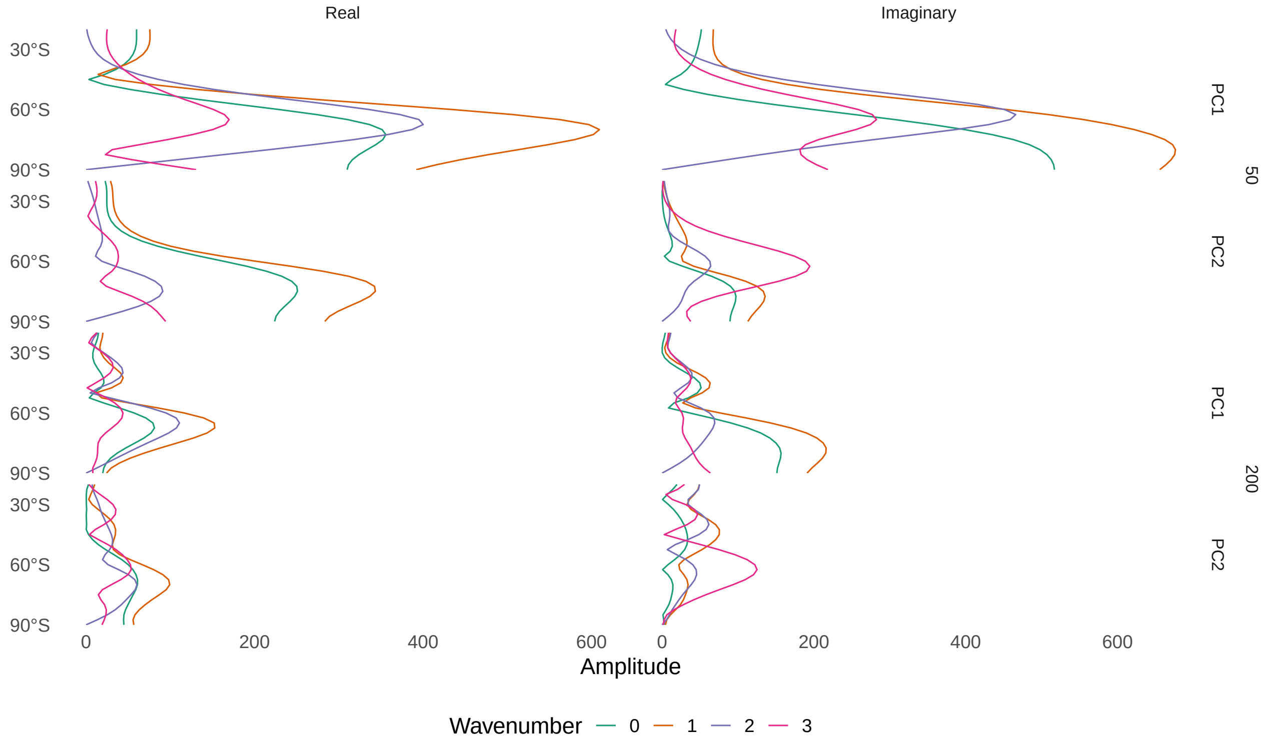

Figure 5: Amplitud de ondas zonales de la regresión con altura geopotencial (figuras anteriores)

- EOF2: PSA1 y PSA2.

- Parte imaginaria: proyecta sobre la parte asimétrica del SAM (PSA2)
- Parte real: relativamente independiente del SAM

El primer EOF es esencialmente una medida de la variabilidad proyectada en la dirección el campo medio. La parte importante, de todas formas, es la Real.

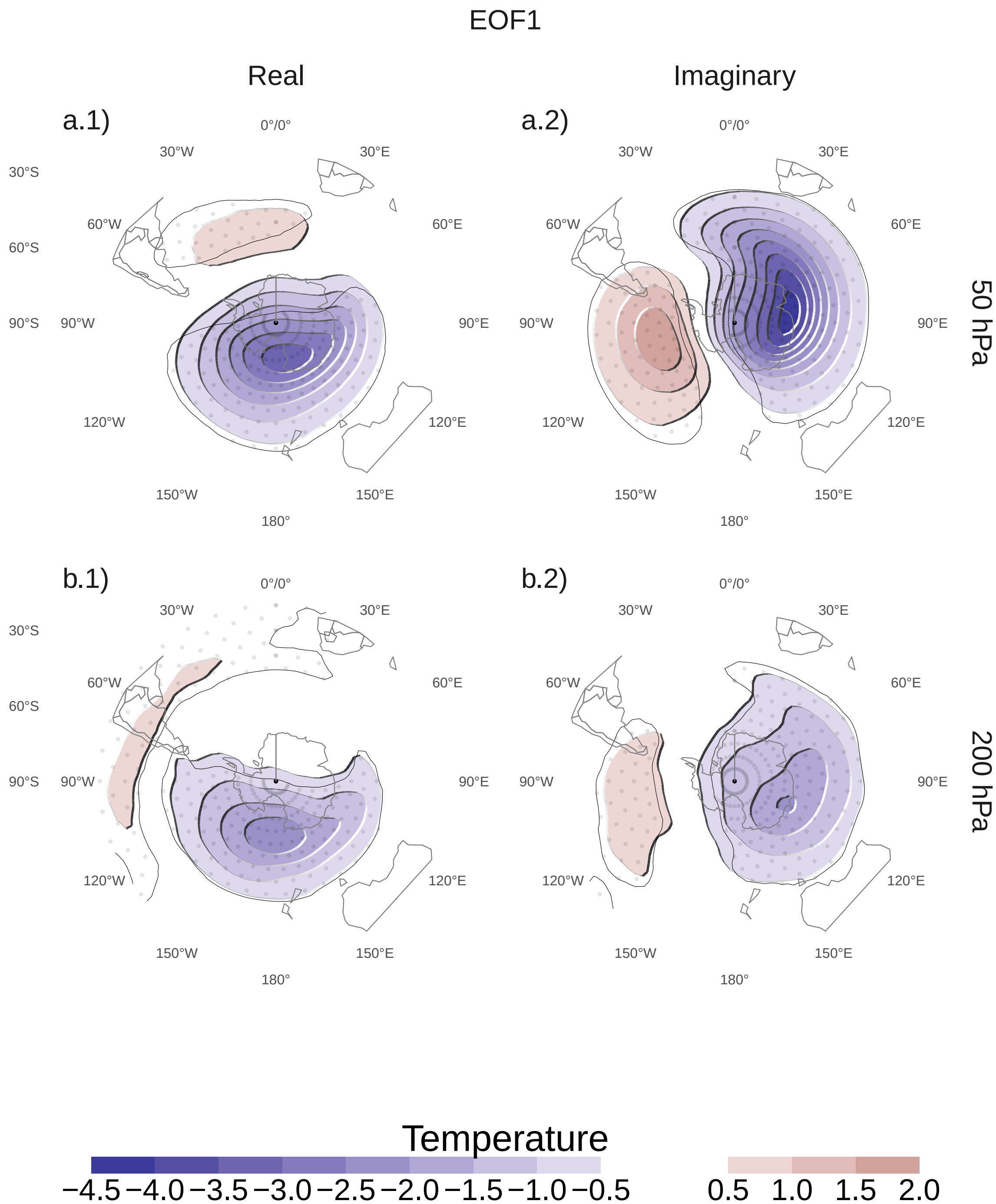

Figure 6: Same as Figure 3 but for air temperature.

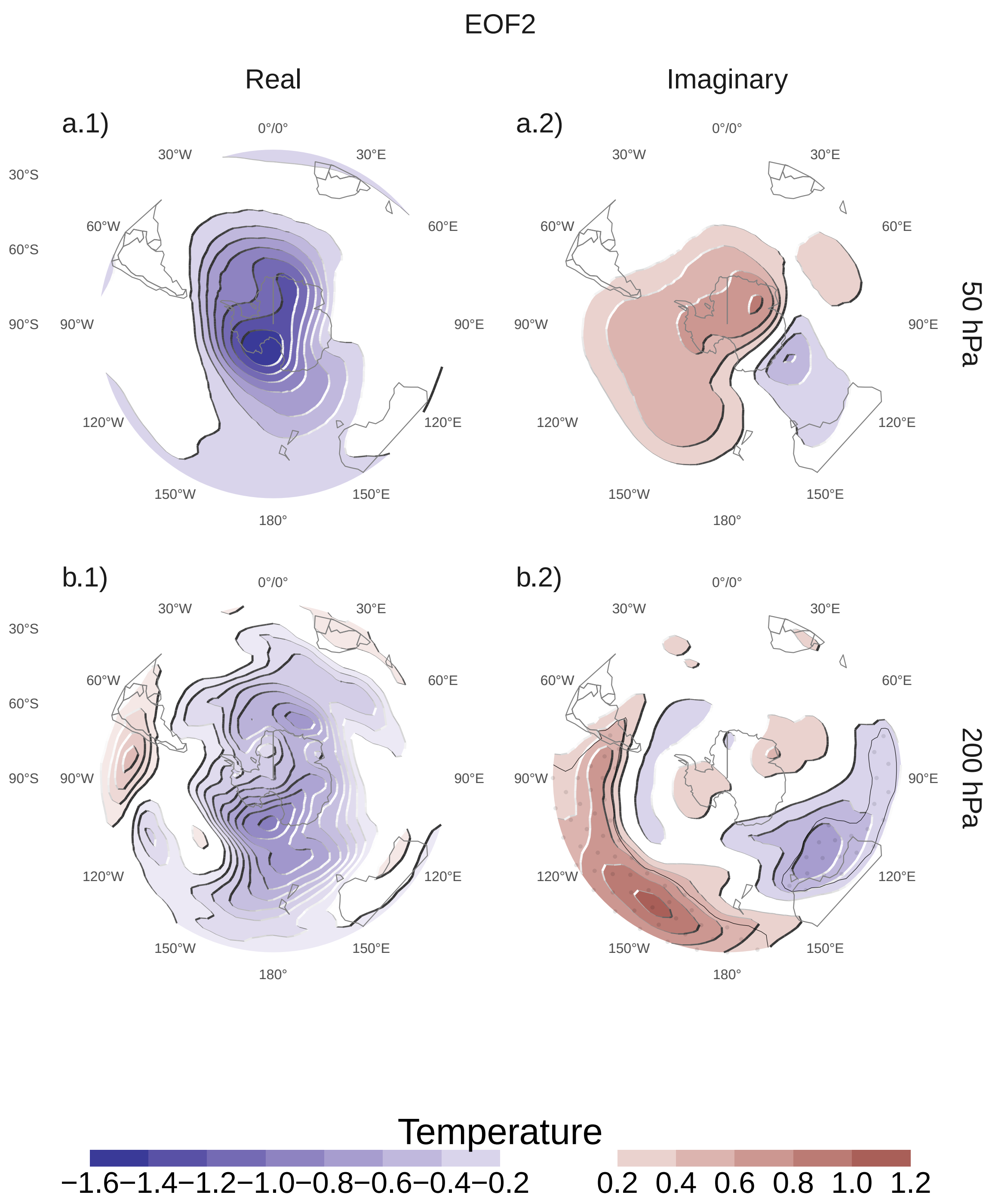

Figure 7: Same as Figure 3 but for the second EOF and temperature.

3.2 Relationship with other indices

3.2.1 PSA1 and PSA2

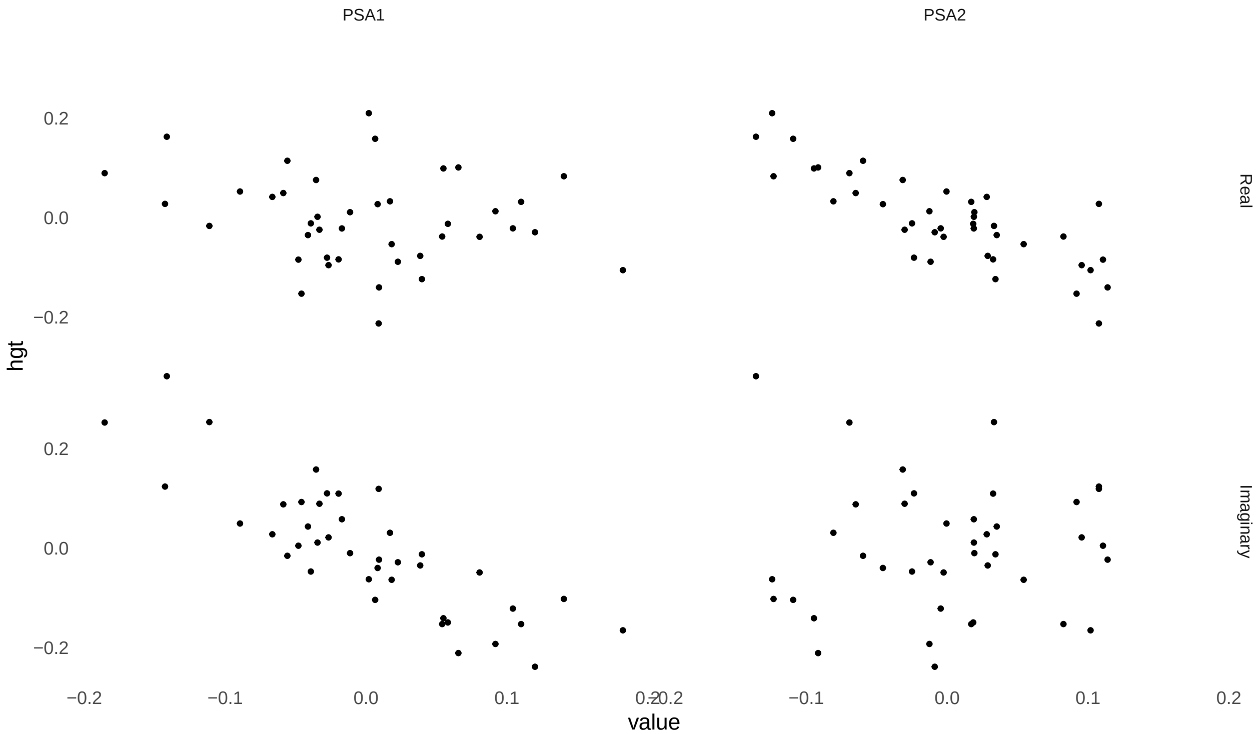

3.2.2 SAM

Figure 8 shows the coefficient of determination between the EOFs and three SAM indices. The SAM index represents the leading EOF of monthly geopotential height fields south of 20ºS at each level. The A-SAM and S-SAM indices represent, respectively, the zonally asymmetric and symmetric component of the SAM and are obtained by projecting the zonally asymmetric and zonally symmetric part of the SAM spatial pattern onto monthly geopotential height fields (Campitelli et al. (2021)). Since the analysis here is only for the SON trimester, monthly values were averaged across semesters (weighted by the number of days in each month).

Both EOFs bear some modest relationship with the SAM index (thick green line in Figure 8), although not statistically significant at every level. The split between A-SAM and S-SAM gives more insight into the nature of the relationship. The relationship between the SAM and the imaginary EOF1 (Figure 8.b1) is mediated by S-SAM in the troposphere, but by the A-SAM in the stratosphere.

The Imaginary EOF2 is related with the SAM through the A-SAM in the troposphere, with up to -96% of shared variance, reached at 225 hPa (Figure 8.b2).

As a further illustration, Figure 9 shows the spatial pattern of the leading EOF of 200 hPa geopotential height when the variability associated with EOF2 is removed. The resulting pattern is an nearly zonally symmetrical annular mode. This mode is highly correlated with SAM (0.75 (CI: 0.58 – 0.86)), but only with the symmetrical part (0.88 (CI: 0.79 – 0.94)). Note that the usual definition of the PSA modes as the second and third EOFs creates modes orthogonal to the SAM (defined as the first EOF) and thus impedes this kind of filtering.

This suggests that the separation between the asymmetric and symmetric part of the SAM is not only statistically possible, but physically plausible. The asymmetric part of the SAM might be statistical contamination from one phase of the PSA mode.

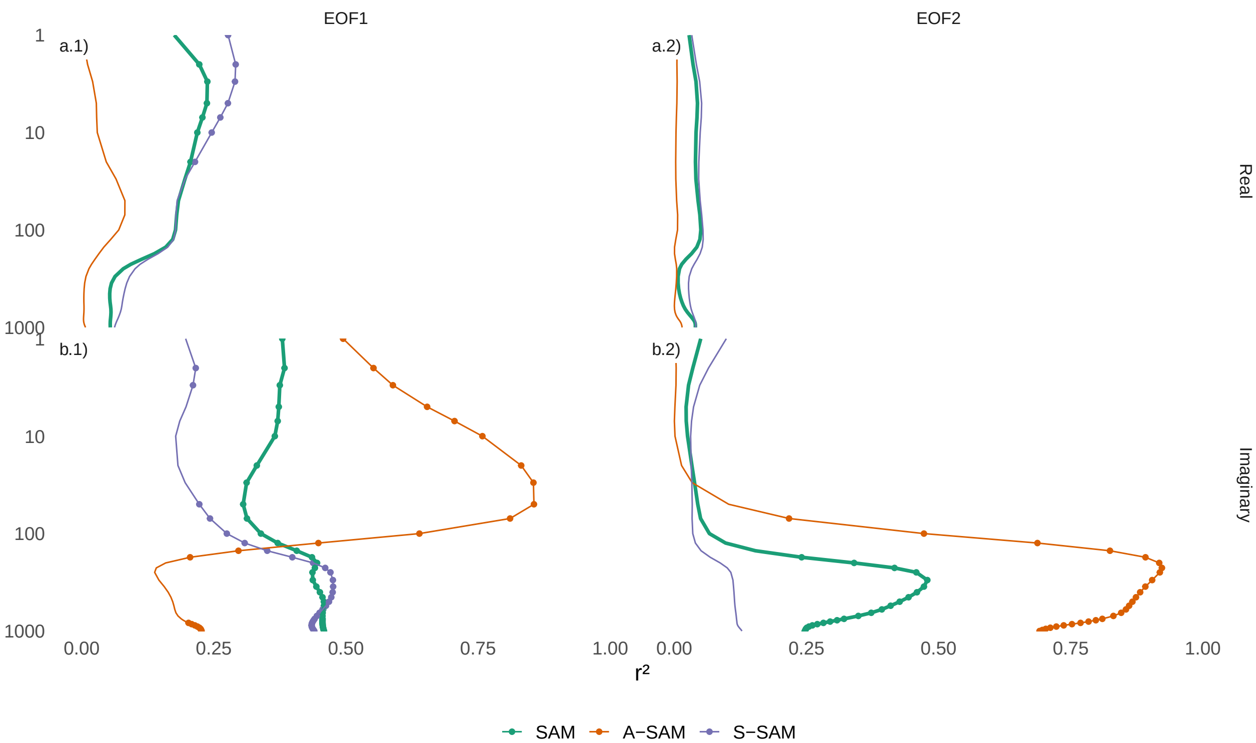

Figure 8: Coefficient of determination between the real and imaginary part of each EOF and the SAM, Asymmetric SAM (A-SAM) and Symmetric SAM (S-SAM) indices computed at each level according to Campitelli et al. (2021). Points mark estimates with p-value < 0.01 corrected for False Detection Rate (Benjamini and Hochberg, 1995).

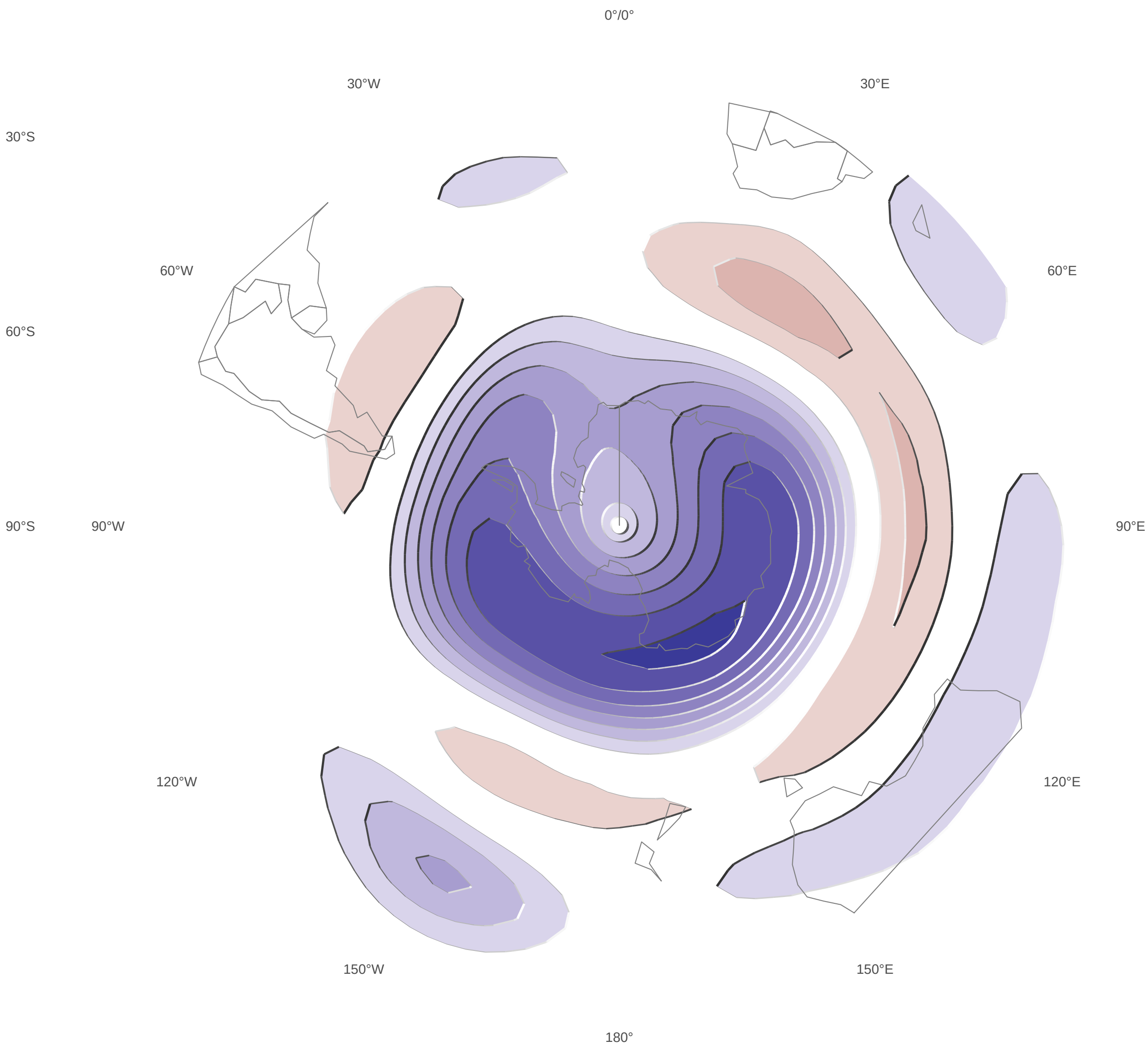

Figure 9: Spatial pattern of the leading EOF of 200 hPa geopotential height with the variability of EOF2 filtered out South of 20º. Arbitrary scale.

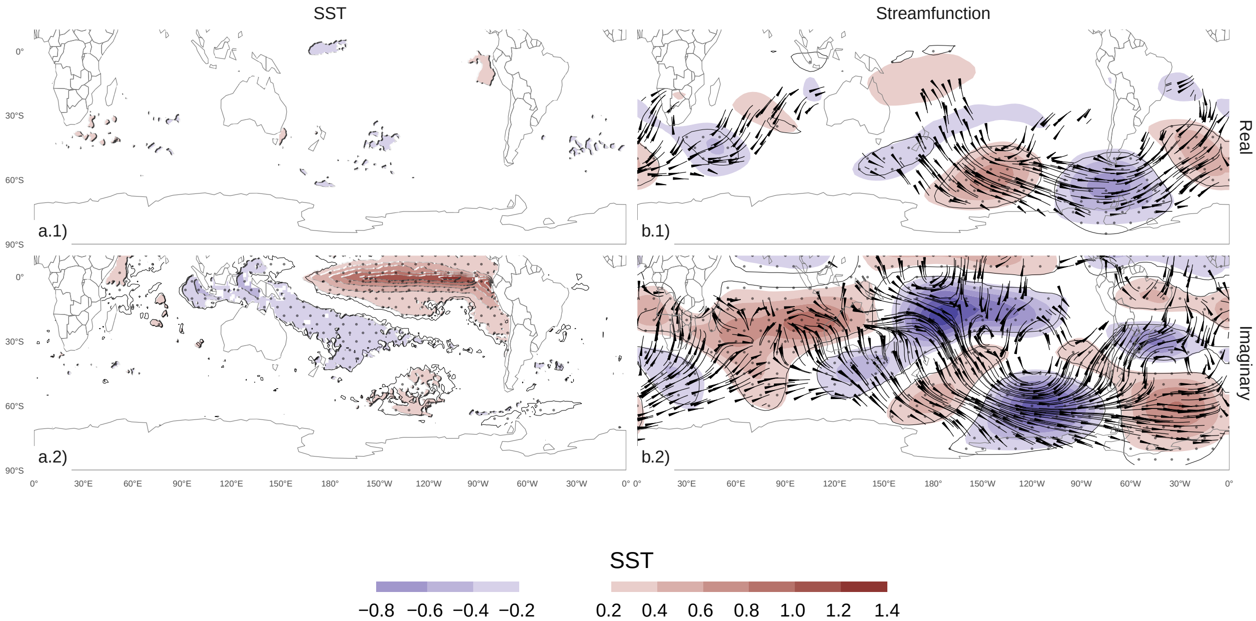

Figure 10: Regression maps of EOF2 with SST (column a) and streamfunction zonal anomalies with their corresponding activity wave flux (column b). Areas marked with dots have p-values smaller than 0.05 adjusted for FDR.

Figure 10 shows regression maps between EOF2 and Sea Surface Temperatures (SST) Streamfunction at 200 hPa. The Imaginary EOF2 is associated with strong positive SST anomalies on the Central Pacific and negative anomalies on an area across the North of Australia and New Zealand, the South Pacific Convergence Zone (SPCZ) (Figure 10.a2). This pattern is almost canonically positive ENSO and indeed, the correlation between the Imaginary EOF2 and the Oceanic Niño Index ((Bamston et al., 1997)) is very high 0.76 (CI: 0.59 – 0.86). Streamfunction anomalies show a coherent picture. The Imaginary EOF2 is associated with strong wave-like streamfunction anomalies emanating from the tropics (Figure 10.b2). This is consistent with what we know of the effect of ENSO on the extratropics: SST anomalies initiate anomalous convection that excites Rossby waves that propagate meridionally towards higher latitudes.

?? Compare with Figura 1 b and c (Streamfunction) and Figure 2 d and FIgure 3 d (SST) from (Mo and Paegle, 2001) and Figure 7 (Irving and Simmonds, 2016).

Imaginary more global than real -> is that why it appears mixed with SAM?

Since the Real EOF2 represents just a different phase of the same wave train, one would expect that it would show a similar forcing pattern to the Imaginary EOF with a slight translation of its location. However, Figure 10.a1 and b1 show that the Real EOF2 is not associated either with any significant SST nor streamfunction anomalies in the tropics. The correlation between the Real EOF2 and ENSO is also not significant (). This lack of tropical signal suggests a radically different nature of the different phases of the EOF2 wave train.

To better explore the relationship between tropical forcing and phase of the EOF2, Figure 11 plots the ONI index and the phase of the EOF2 for each year between 1979 and 2019, highlighting years in which the magnitude of EOF2 was higher than 50% of the years. In years with positive ENSO, the phase of the EOF2 is always around $+90^{o}$ (corresponding with positive imaginary part) and vice versa. In years with near neutral ENSO, the phase of the EOF2 is much more variable. The black line in Figure 11 tries to quantify this relationship. Is the equation $ONI = 1.1 \sin phase$, whose coefficient we fitted by weighted least squares using the magnitude of the EFO2 as weight. The r^2 corresponding to the fit is 0.56, with p-value < 0.001.

Figure 11 suggest that strong EOF2 years tend to coincide with strong ENSO years. The correlation between the absolute magnitude of the ONI and the magnitude of the EOF2 is 0.44 (CI: 0.16 – 0.66). This relationship appears to be driven only by the three years with strongest ENSO events in the period (2015, 1997, and

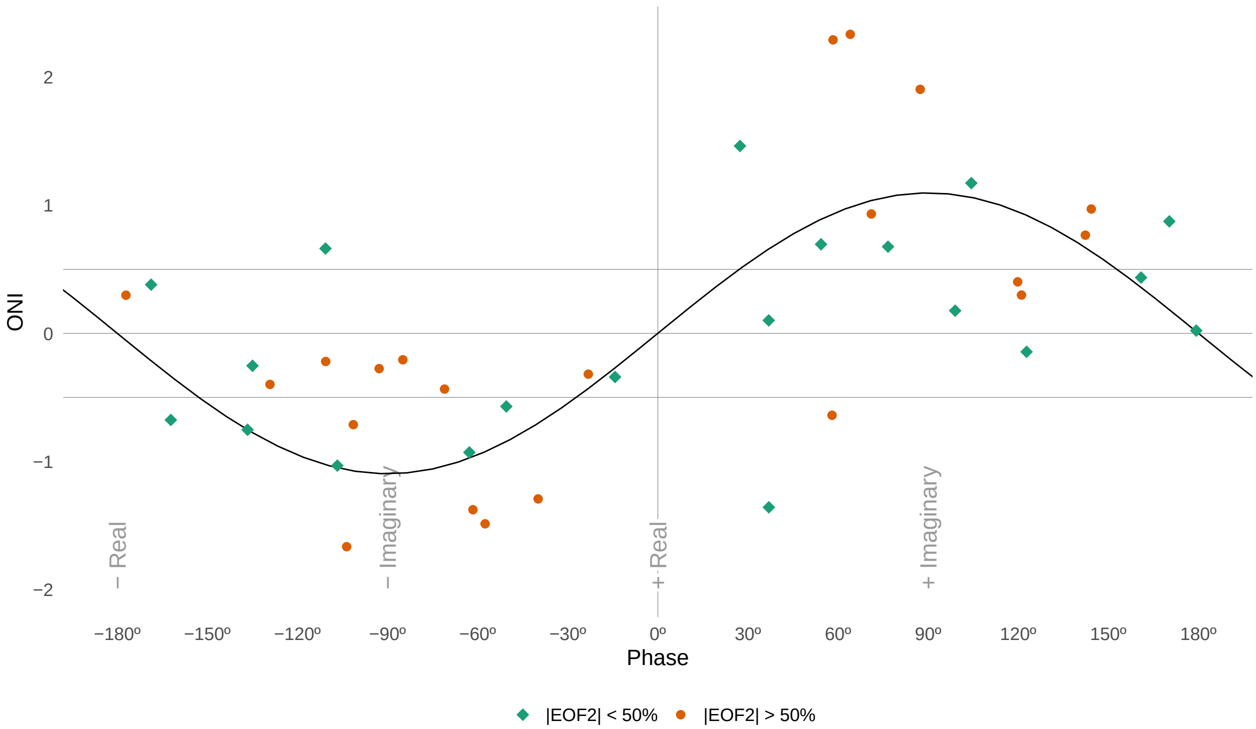

Figure 11: Relationship between ENSO and phase of EOF2 for the period 1979 – 2019. Colours denote years with magnitude of EOF2 greater or smaller than the 50th percentile. Black line is the fit ONI ~ cos(phase) + sin(phase) computed by OLS weighted by the magnitude of EOF2.

1982) which also coindice with the three years with strongest EOF2 magnitude. If those years are removed, the correlation becomes non-significant (0.044 (CI: -0.28 – 0.36)). Furthermore, the Spearman correlation, which is robust to outliers is also non-significant (0.2, p-value = = 0.2). Therefore, the relationship between the magnitude of the EOF2 train wave and ENSO remains uncertain.

All this suggests that the wave train represented by EOF2 can be both forced by tropical SSTs and also a part of the internal variability of the extratropical atmosphere. When internally forced, the wave train has little phase preference. When excited by tropical SST anomalies, it tends to remain locked to the imaginary phase, with the sign of the geopotential anomalies depending on the sign of the tropical SSTs anomalies.

Figure 12 shows SST and streamfunction regression maps for EOF1. There is no significant pattern of SST anomalies associated with either the Real or Imaginary EOF1. Consistently, streamfunction anomalies don't show any tropical influence. On the contrary, the Real EOF1 is associated with wave activity fluxes that flow equatorward from the coast of Antarctica around 150ºE along with wave activity fluxes that move between the positive and negative of Streamfunction anomalies along Antarctica.

3.3 Precipitation

Figure 13 shows regression maps of seasonal precipitation with each EOF in South America. EOF1 (Figure 13 column a) is associated with increased precipitation over Paraguay and and some parts of Brazil. Although these positive anomalies are not very strong. The strongest precipitation anomalies are the ones associated with the Imaginary EOF2. The positive anomalies on Southeaster South America (SESA) and Chile, and negative anomalies over Southern Brazil is a well known springtime precipitation signature of ENSO (Cai et al., 2020) and it's also virtually identical to the precipitation anomalies associated with the Asymmetric SAM (Campitelli et al., 2021). This is not surprising considering the close relationship between the ONI, the Asymmetric SAM index and the Imaginary EOF2 shown previously. The Real EOF2, on the other hand,

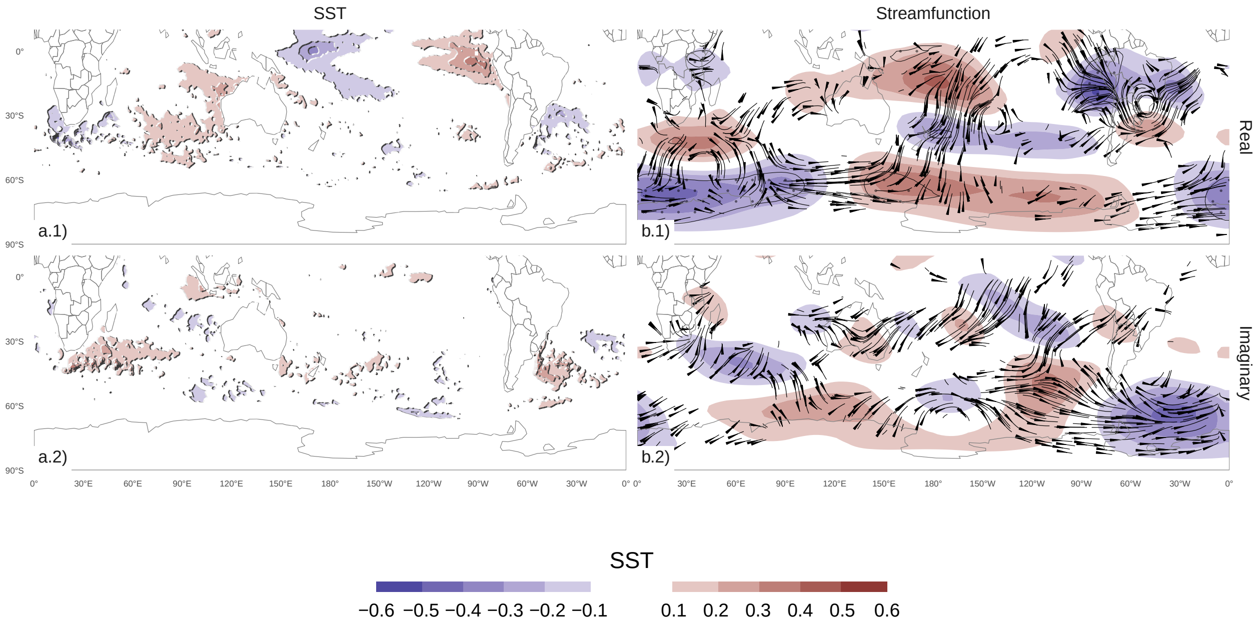

Figure 12: Same as Figure 10 but for EOF1.

is associated with negative precipitation anomalies in a smaller area of SESA. The relationship between precipitation anomalies in SESA and the phase of EOF2 follows a curve similar to that of Figure 11 (not shown).

4 Conclusions

5 Appendix

5.1 Naive EOFs

5.2 Chosen rotations of the EOFs

6 References

Bamston, A.G., Chelliah, M., Goldenberg, S.B., 1997. Documentation of a highly ENSO-related sst region in the equatorial pacific: Research note. Atmosphere-Ocean 35, 367–383. https://doi.org/10.1080/07055900.1997.9649597

Benjamini, Y., Hochberg, Y., 1995. Controlling the False Discovery Rate: A Practical and Powerful Approach to Multiple Testing. Journal of the Royal Statistical Society: Series B (Methodological) 57, 289–300. https://doi.org/10.1111/j.2517-6161.1995.tb02031.x

Cai, W., McPhaden, M.J., Grimm, A.M., Rodrigues, R.R., Taschetto, A.S., Garreaud, R.D., Dewitte, B., Poveda, G., Ham, Y.-G., Santoso, A., Ng, B., Anderson, W., Wang, G., Geng, T., Jo, H.-S., Marengo, J.A., Alves, L.M., Osman, M., Li, S., Wu, L., Karamperidou, C., Takahashi, K., Vera, C., 2020. Climate impacts of the El NiñoSouthern Oscillation on South America. Nature Reviews Earth & Environment 1, 215–231. https://doi.org/10.1038/s43017-020-0040-3

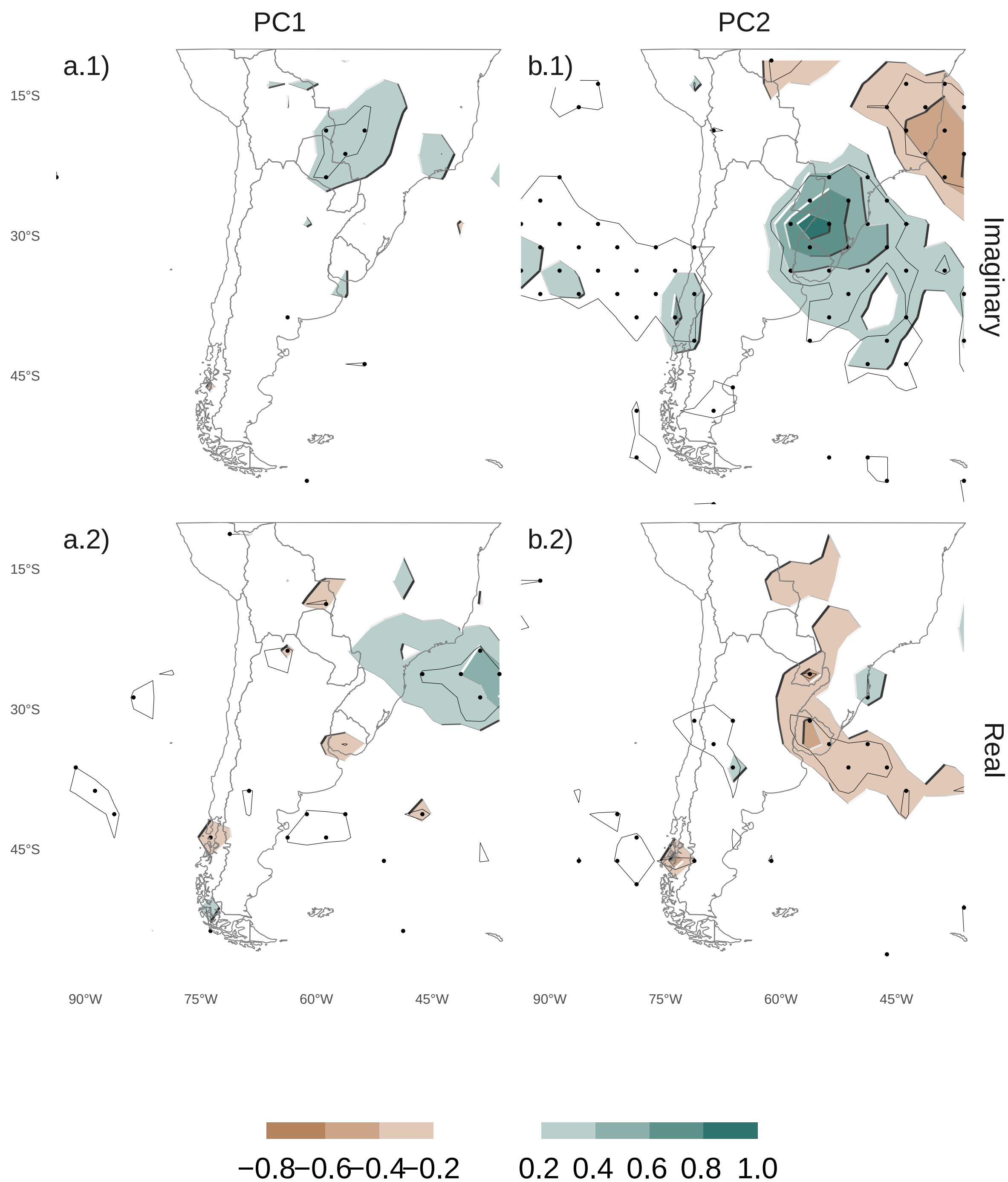

Figure 13: Regression of SON mean precipitation anomalies in South America (mm per day, shaded) and (column a) EOF1 the (row 1) Imaginary and (column 1) Real phase. For the 1979 – 2018 period. Black contours with dots indicate areas with p-value smaller than 0.05 controlling for False Detection Rate.

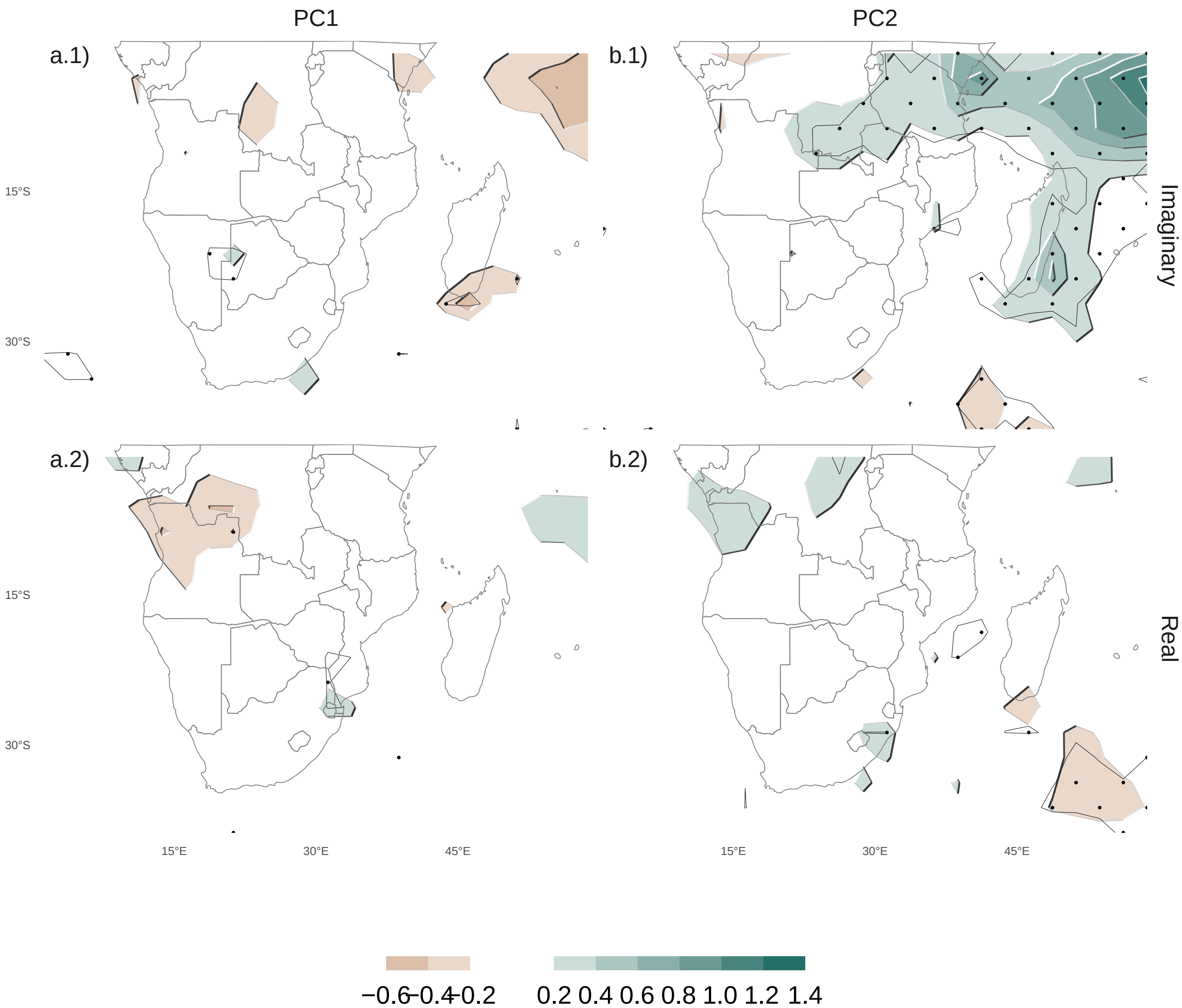

Figure 14: Same as Figure 13 but for South of Africa.

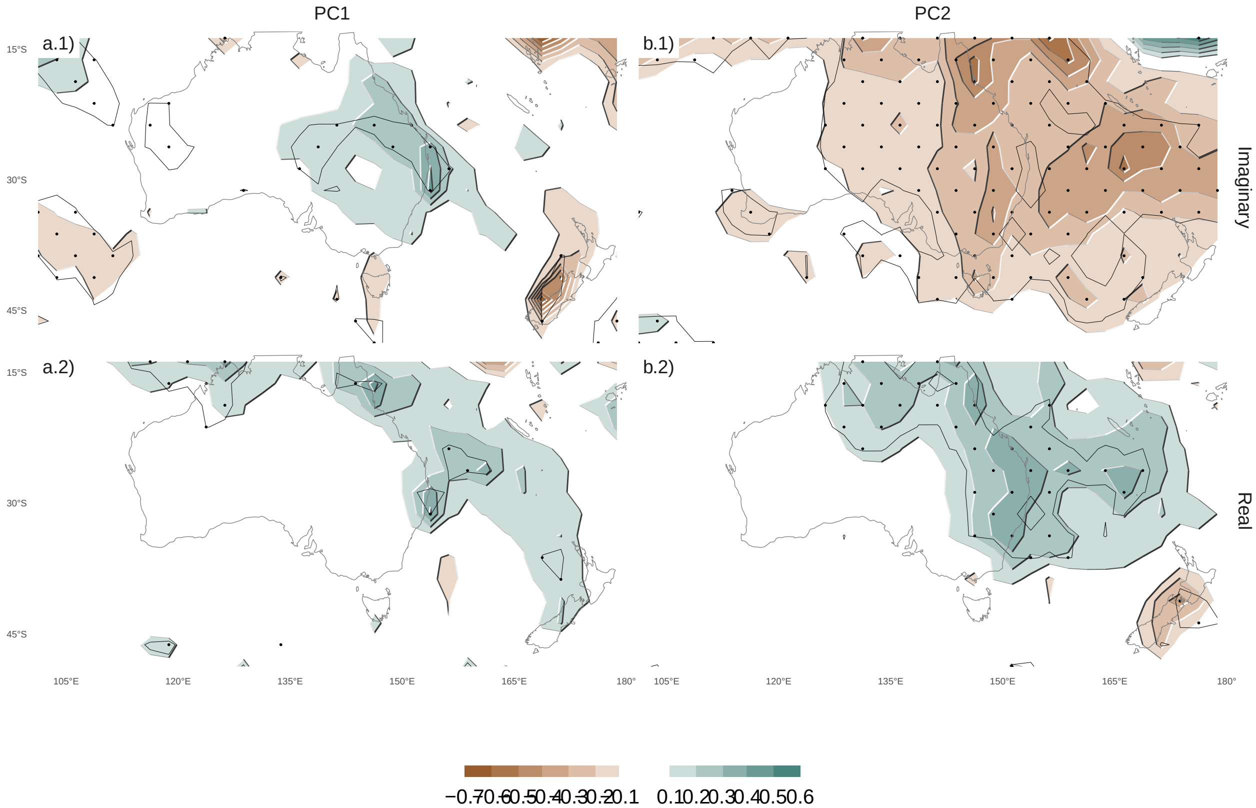

Figure 15: Same as Figure 13 but for New Zealand and neighbouring islands.

Campitelli, E., Diaz, L., Vera, C., 2021. Assessment of zonally symmetric and asymmetric components of the Southern Annular Mode using a novel approach. Climate Dynamics (under review).

Horel, J.D., 1984. Complex Principal Component Analysis: Theory and Examples. Journal of Applied Meteorology and Climatology 23, 1660–1673. https://doi.org/10.1175/1520-0450(1984)023%3C1660:CPCATA%3E2.0.CO;2

Irving, D., Simmonds, I., 2016. A New Method for Identifying the PacificSouth American Pattern and Its Influence on Regional Climate Variability. Journal of Climate 29, 6109–6125. https://doi.org/10.1175/JCLI-D-15-0843.1

Mo, K.C., Paegle, J.N., 2001. The PacificSouth American modes and their downstream effects. International Journal of Climatology 21, 1211–1229. https://doi.org/10.1002/joc.685

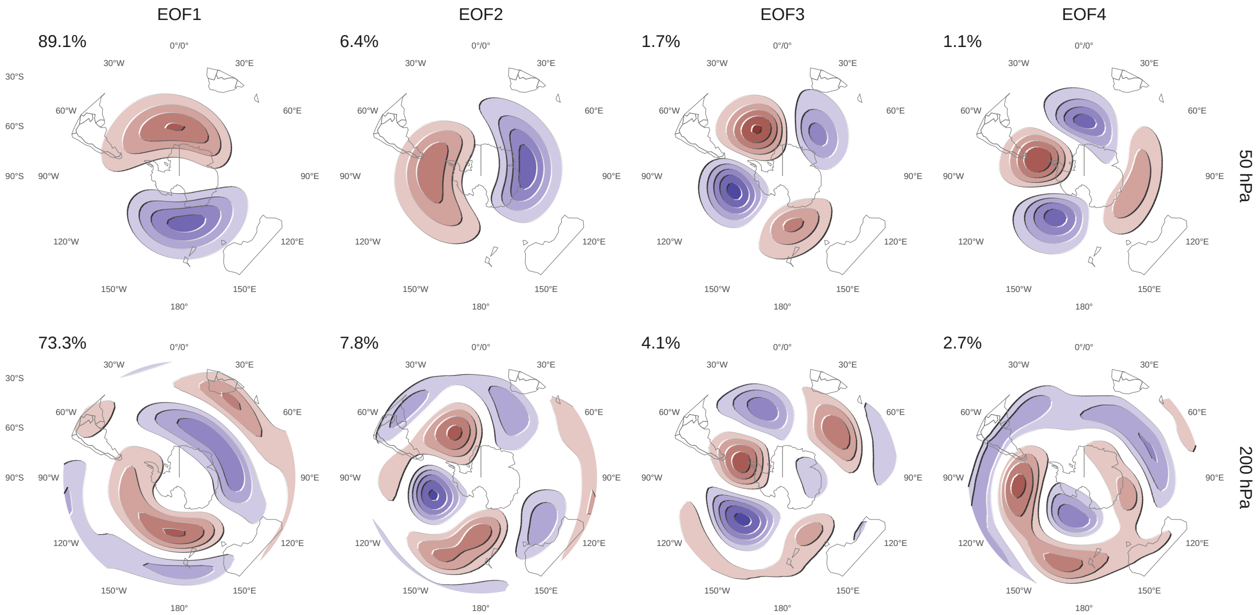

(a) Spatial patterns (arbitrary units). The numbers at the top-left of each panel is the variance explained by each EOF.

(b) Coefficient of determination of the temporal index of each EOF between levels.

Figure 16: Leading 4 EOFs of zonal anomalies of geopotential height at 50 hPa and 200 hPa for the SON trimester and the period 1979 – 2009.

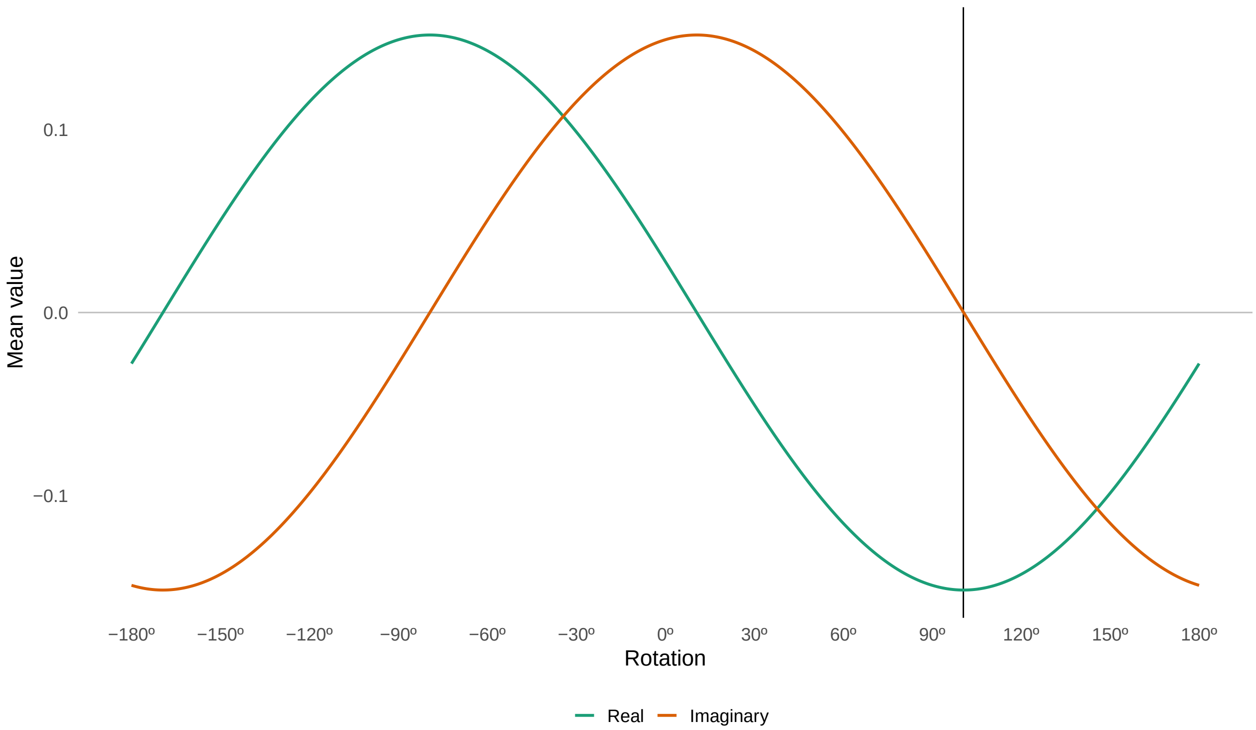

Figure 17: Rotations of PC1

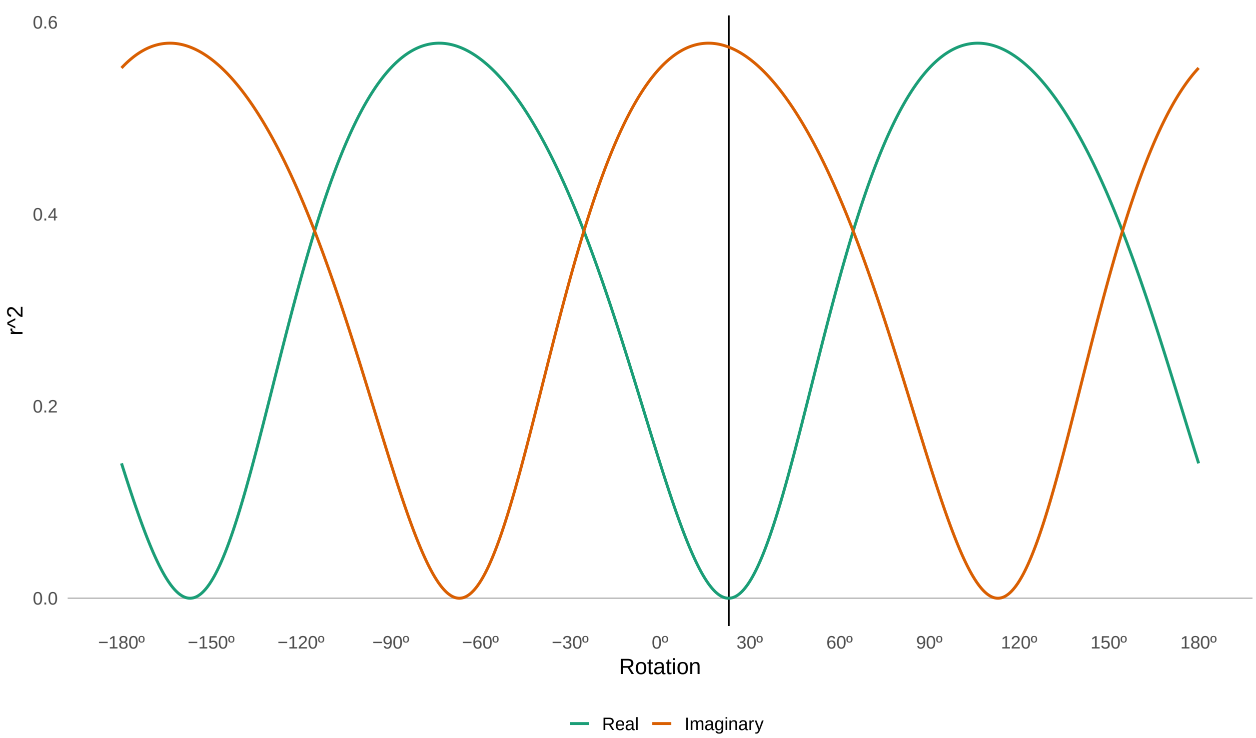

Figure 18: R2 between EOF2 Real and Imaginary parts and ONI index for different rotation parameters of the real and imaginary parts.